

1 **Structural Design of Self-thermal Methanol Steam Reforming Microreactor with**
2 **Porous Combustion Reaction Support for Hydrogen Production**

3 Tianqing Zheng^a, Wei Zhou ^{a*}, Xinying Li^a, Huihui You^a, Yifan Yang^a, Wei Yu^a,
4 Chenying Zhang^a, Xuyang Chu ^{a*}, Kwan San Hui^b, Weihua Ding^c

5 ^a *Department of Mechanical & Electrical Engineering, Xiamen University, Xiamen 361005, China*

6 ^b *School of Mathematics, University of East Anglia, Norwich, NR4 7TJ, United Kingdom*

7 ^c *Rison Hi-tech Materials Company Limited, Yiwu 322000, China*

8 **Abstract:** To replace the traditional electric heating mode and increase methanol
9 steam reforming reaction performance in hydrogen production, methanol catalytic
10 combustion was proposed as heat-supply mode of methanol steam reforming
11 microreactor. Moreover, the methanol catalytic combustion microreactor and
12 self-thermal methanol steam reforming microreactor for hydrogen production were
13 developed. Furthermore, catalytic combustion reaction supports with different
14 structures were designed. It was found that the developed self-thermal methanol steam
15 reforming microreactor had better reaction performance. Compared with A-type, the
16 ΔT_{\max} of C-type porous reaction support was decreased by 24.4°C under 1.3 mL/min
17 methanol injection rate. Moreover, methanol conversion and H₂ flow rate of the
18 self-thermal methanol steam reforming microreactor with C-type porous reaction
19 support were increased by 15.2% under 10 mL/h methanol-water mixture injection
20 rate and 340 °C self-thermal temperature. Meanwhile, the CO selectivity was
21 decreased by 4.1%. This work provides a new structural design of the self-thermal
22 methanol steam reforming microreactor for hydrogen production for the fuel cell.

23 **Keywords:** Microreactor for hydrogen production; Self-thermal reaction; Porous
24 reaction support; Thermal distribution

25 *Corresponding author. Tel.: 86-592-2188698; Fax: 86-592-2186383

26 E-mail address: chuxy@xmu.edu.cn (Xuyang Chu), weizhou@xmu.edu.cn (Wei Zhou).

1. Introduction

The technology of hydrogen production by methanol steam reforming microreactor was used as one of the preferred hydrogen production technologies because of its advantages, such as high hydrogen content, low cost, renewable, safe and efficient^[1-5]. However, electric heating mode was used as the main heat-supply mode of the microreactor^[6-7]. The high power consumption of electric heating mode limited the application of methanol steam reforming microreactor for hydrogen production in the fuel cell, especially in the mobile power station using fuel cell^[8].

The solar energy, methanol combustion and butane combustion used as the heat-supply mode for methanol steam reforming microreactor for hydrogen production had been investigated by some scholars^[9-13]. For example, Gu *et al.* designed and manufactured a small portable condenser collector to supply heat for the methanol reforming process for hydrogen production^[9]. Chein *et al.* developed a methanol steam reforming microreactor for hydrogen production with the combustion chamber, which used methanol catalytic combustion to supply heat for methanol steam reforming for hydrogen production^[10].

However, the above studies emphasized on the application of heat-supply mode in methanol steam reforming reaction. The thermal distribution of the exothermic reaction plate for different heat-supply modes has not been systematically investigated. The reaction performance of the catalyst for methanol steam reforming for hydrogen production was affected by the thermal distribution of the microreactor^[6, 14]. In this way, the methanol steam reforming reaction performance in hydrogen production was

Nomenclature

Variables

m volume proportion of CO in reaction gas, %

n volume proportion of CO₂ in reaction gas, %

S_{co} the selectivity of CO in reaction gas, %

V_{H_2} flow rate of H₂, mol/h

$V_{\text{injection}}$ injection velocity of the methanol-water mixture, mL/h

$V_{\text{reaction gas}}$ injection velocity of reaction gas, mL/min

$X_{\text{CH}_3\text{OH}}$ methanol conversion, %

z volume proportion of H₂ in reaction gas, %

Abbreviations

PPI pores per inch

ΔT_{max} the maximum temperature difference of thermal distribution

49

50 related to the thermal distribution of the microreactor. Therefore, it was necessary to
51 study the thermal distribution of the heat-supply process.

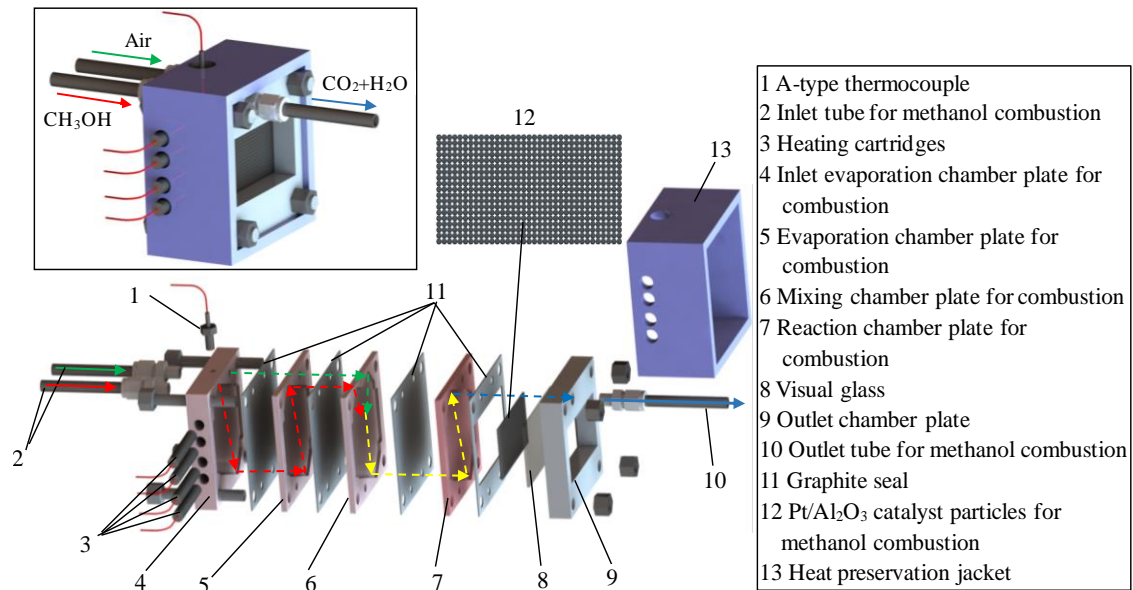
52 In fact, studies on the thermal distribution of exothermic reaction plate which
53 was heat-supplied by different heat-supply technologies have been investigated by a
54 few research groups^[12-13]. For example, Hsueh *et al.* used numerical simulations to
55 investigate the mass-transfer and heat-transfer performances of the plate-type
56 methanol steam reforming microreactor coupled with methanol combustor. It was
57 found that it increased the methanol steam reforming reaction performance in
58 hydrogen production if the flow direction relationship between methanol steam
59 reforming gas and the methanol catalytic combustion gas flow was opposite^[12].
60 Herdem *et al.* used numerical simulations to study the thermal distribution of

61 microchannel methanol steam reformer. They found that the methanol steam
62 reforming reaction performance in hydrogen production can be increased using the
63 reaction plate with reasonable thermal distribution^[13].

64 Although some studies on the reaction performance and thermal distribution of
65 methanol steam reforming microreactor with different heat-supply modes for
66 hydrogen production have been carried out, the structural design and the thermal
67 distribution optimization of the self-thermal methanol steam reforming microreactor
68 for hydrogen production have not been systematically reported in previous studies.
69 The reasonable thermal distribution of reaction plate was beneficial for increasing the
70 reaction performance of the methanol steam reforming microreactor for hydrogen
71 production. Therefore, combined with the our previous research works of the
72 methanol steam reforming microreactor^[6-7,15], to promote the industrial application of
73 the microreactor and increase the reaction performance of the microreactor, a
74 methanol catalytic combustion microreactor and a self-thermal methanol steam
75 reforming microreactor for hydrogen production were firstly developed using
76 methanol catalytic combustion as the heat-supply mode. Then, the catalytic
77 combustion reaction supports with different structures were designed to optimize the
78 thermal distribution. Moreover, the thermal distribution of the different reaction
79 supports was analyzed in detail using the infrared thermal imager and temperature
80 inspector. Furthermore, the reaction performance of the self-thermal methanol steam
81 reforming microreactor with the different reaction supports was compared and
82 discussed.

83 2. Experimental Methods

84 2.1 Structural design of methanol catalytic combustion microreactor



85

86

Fig.1. Structural diagram of the methanol catalytic combustion microreactor

87

Fig.1 shows the structural diagram of the methanol catalytic combustion

88

microreactor. This microreactor used for combustion consisted of inlet evaporation

89

chamber plate, evaporation chamber plate, mixing chamber plate, and reaction

90

chamber plate for combustion; in addition, it contained a visual glass, an outlet

91

chamber plate and a heat preservation jacket. The inlet chamber plate and evaporation

92

chamber plate for combustion were used to convert the liquid methanol into gaseous

93

methanol. The mixing chamber plate for combustion was used to mix methanol and

94

air. The reaction chamber plate for combustion with a 70 mm × 40 mm × 2 mm

95

chamber was filled with catalytic combustion reaction support. The visual glass was

96

set in the outlet chamber plate, and it was used to observe the methanol catalytic

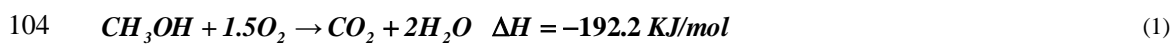
97

combustion reaction in the reaction chamber plate for combustion. The heat

98

preservation jacket was used to preserve heat in the microreactor.

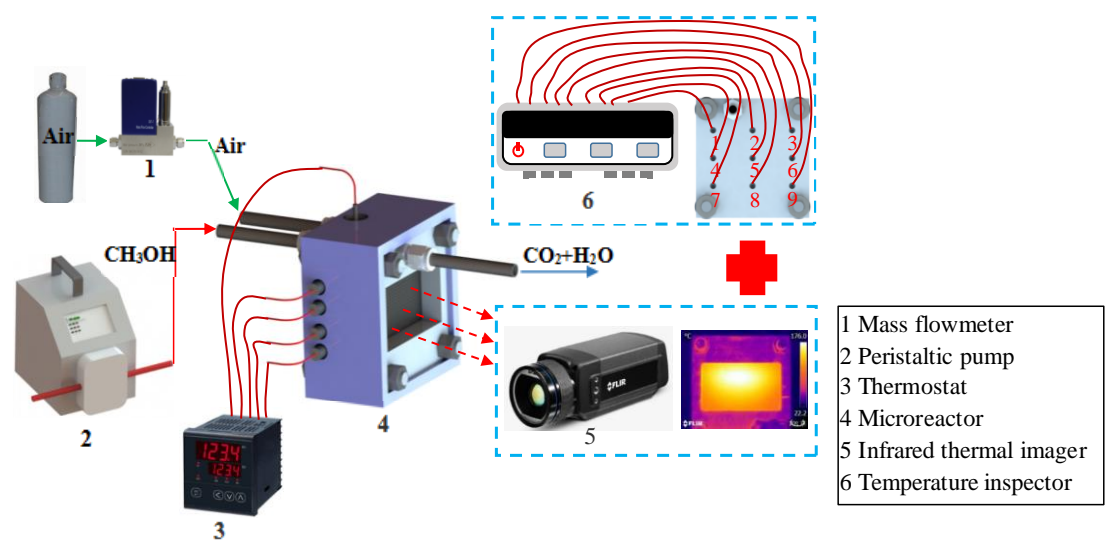
99 Liquid methanol was gasified through the inlet evaporation chamber plate and
100 evaporation chamber plate for combustion, and it was subsequently mixed with air in
101 the mixing chamber plate for combustion. Then, the mixed gas was reacted with the
102 catalyst which was in the reaction chamber plate for combustion. Eq. (1) indicates the
103 reaction process for methanol catalytic combustion reaction^[16-19].



105 **2.2 Construction of testing system for the methanol catalytic combustion** 106 **microreactor**

107 Fig.2 shows a structural diagram of the testing system for the methanol catalytic
108 combustion microreactor. The testing system mainly consisted of compressed air
109 bottle, mass flowmeter (D07-7B, Beijing Sevenstar Electronics Company, China),
110 peristaltic pump (BT300S, Baoding Lead Fluid Company, China), microreactor,
111 thermostat, heating cartridges, A-type thermocouple, infrared thermal imager (FLIR
112 T440, FLIR Systems Company, USA), and temperature inspector (AT4516, Applent
113 Instruments Company, China). Methanol was injected into the microreactor using a
114 peristaltic pump. Air was supplied into microreactor by air bottle and mass flowmeter.
115 The heating cartridges and A-type thermocouple on the inlet evaporation chamber
116 plate for combustion and thermostat were used to perform the preheat of the
117 microreactor before the heat-supply by the methanol catalytic combustion reaction for
118 the microreactor itself. The visual glass was set in the outlet chamber plate. The
119 thermal distribution of the reaction chamber plate for combustion was observed using
120 infrared thermal imager. Meanwhile, the thermal distribution of reaction chamber

121 plate for combustion can be investigated using temperature inspector to measure the
 122 temperatures of nine temperature measurement points of the outlet chamber plate.

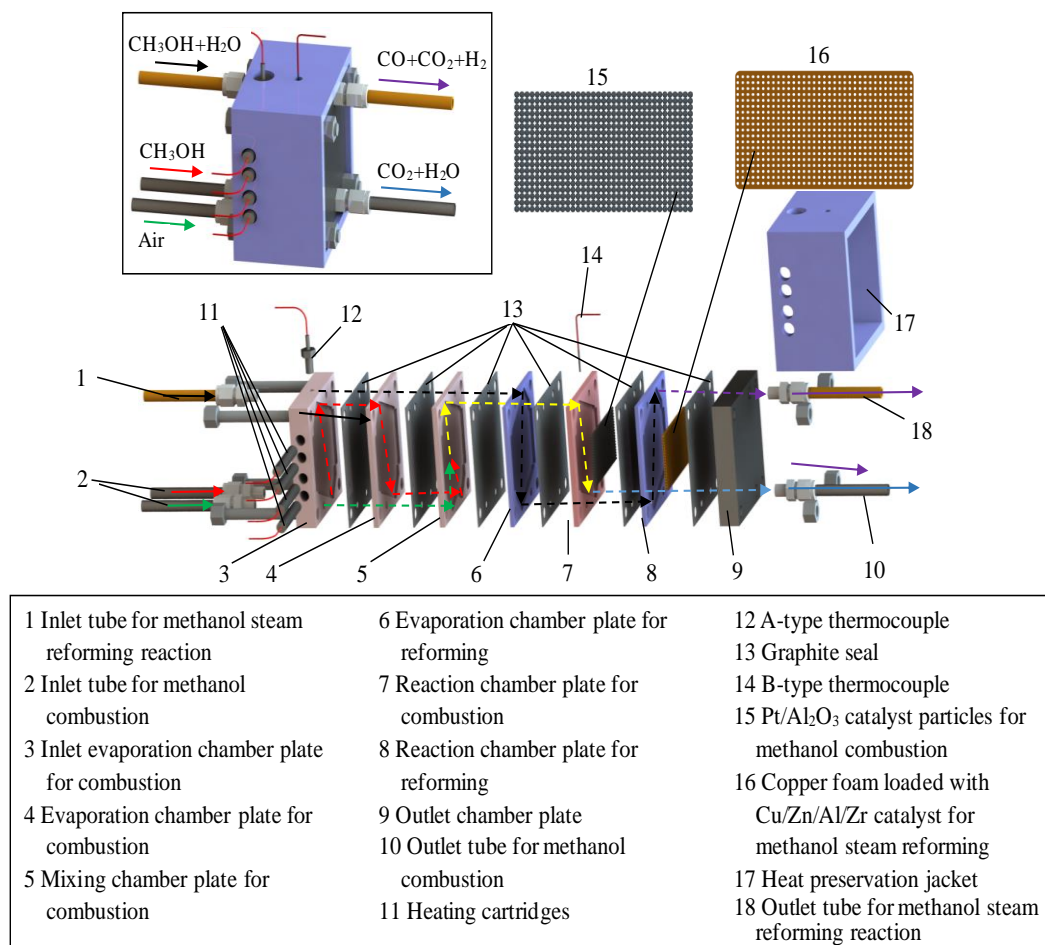


123
 124 Fig.2. Structural diagram of the testing system for the methanol catalytic combustion microreactor

125 Before the occurrence of methanol catalytic combustion reaction, the methanol
 126 catalytic combustion microreactor was preheated by electric heating, and the heating
 127 temperature of thermostat was set to 300 °C. When the temperature on the inlet
 128 evaporation chamber plate for combustion was 300 °C, methanol and air were injected
 129 into the microreactor. Then, when the temperature on the inlet evaporation chamber
 130 plate for combustion was more than 300 °C, the heating temperature of thermostat
 131 was set to 25 °C. In this time, the methanol catalytic combustion microreactor was
 132 heat-supplied by itself. The thermal distribution on the reaction chamber plate for
 133 combustion was used as an index for evaluating the methanol catalytic combustion
 134 reaction performance of the microreactor. The methanol catalytic combustion reaction
 135 performance of the microreactor was measured using an infrared thermal imager and a
 136 temperature inspector. The infrared thermal imager was used to investigate the overall

137 thermal distribution on the reaction chamber plate for combustion^[20-21]. The
 138 temperature inspector was used to investigate the temperature differences between
 139 nine temperature measurement points on the reaction chamber plate for combustion.

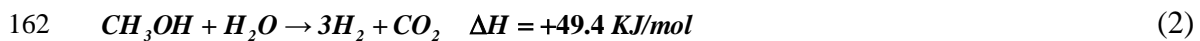
140 **2.3 Structural design of self-thermal methanol steam reforming microreactor for**
 141 **hydrogen production**



142
 143 Fig.3. Structural diagram of the self-thermal methanol steam reforming microreactor
 144 for hydrogen production

145 Fig.3 shows a structural diagram of the self-thermal methanol steam reforming
 146 microreactor for hydrogen production. The microreactor consisted of an inlet
 147 evaporation chamber plate, evaporation chamber plate, mixing chamber, and reaction
 148 chamber plate for combustion, evaporation chamber plate and reaction chamber plate

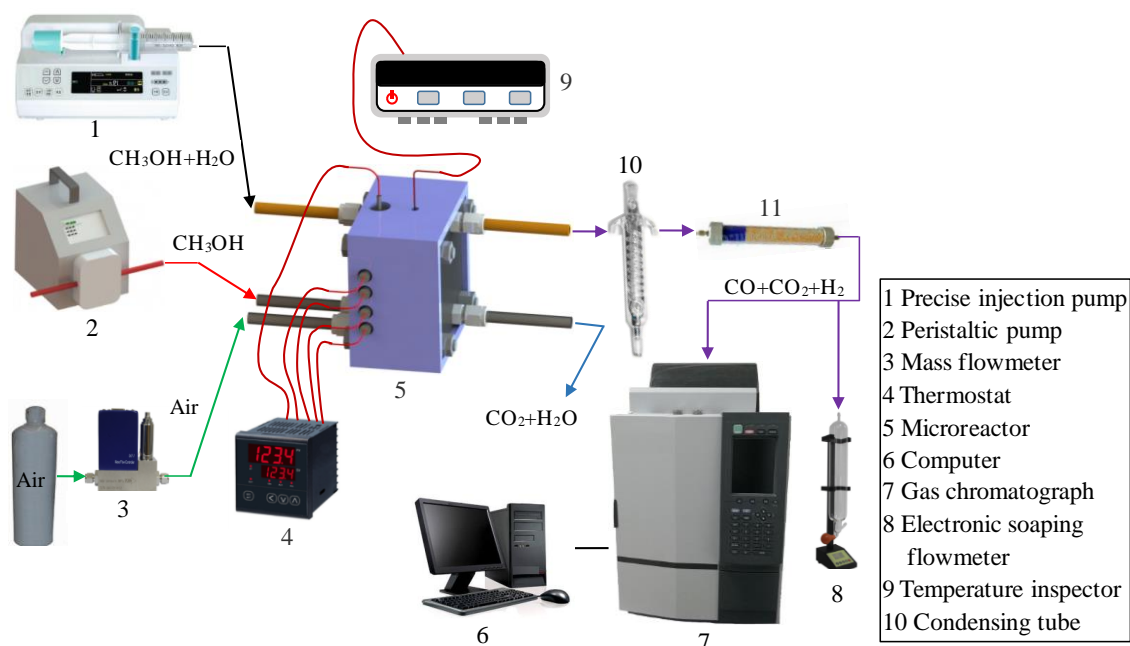
149 for reforming, outlet chamber plate, and heat preservation jacket. Similar to the
150 methanol catalytic combustion microreactor, the inlet evaporation chamber plate,
151 evaporation chamber plate, mixing chamber, reaction chamber plate and the Pt/Al₂O₃
152 catalyst particles were used in the methanol catalytic combustion reaction for
153 combustion^[16-19]. The methanol catalytic combustion reaction in the reaction chamber
154 plate for combustion was used to supply heat to the reaction chamber plate for
155 methanol steam reforming reaction. The flow direction relationship of reaction gas
156 between the reaction chamber plate for combustion and the reaction chamber plate for
157 reforming was opposite. The methanol for reforming was evaporated in the
158 evaporation chamber plate for reforming. The methanol steam reforming gas was
159 reacted with Cu/Zn/Al/Zr catalyst loaded on the copper foam in the reaction chamber
160 plate for reforming^[6,7]. The heat preservation jacket was used to preserve heat in the
161 microreactor.



165 The main reaction process of methanol steam reforming in hydrogen production
166 is shown in Eqs. (2)-(4)^[22-24]. Eq. (2) is the algebraic summation of Eqs. (3) and (4).
167 Eq. (3) indicates the methanol decomposition. Eq. (4) indicates a water–gas shift
168 reaction. The dominant products in the reaction gas are H₂ and CO₂, while a small
169 percentage of CO exists.

170

171 **2.4 Construction of testing system for self-thermal methanol steam reforming**
 172 **microreactor for hydrogen production**



173
 174 Fig.4. Structural diagram of the testing system of the self-thermal methanol steam reforming
 175 microreactor for hydrogen production

176 Fig.4 shows the structural diagram of the testing system of the self-thermal
 177 methanol steam reforming microreactor for hydrogen production. The testing system
 178 consisted of compressed air bottle, mass flowmeter, peristaltic pump, precise injection
 179 pump (JZB-1800, Jianyuan Medical Equipment Company, China), microreactor,
 180 thermostat, heating cartridges, A-type thermocouple, infrared thermal imager, and
 181 temperature inspector, electronic soaping flowmeter (JCL-2010(S)-A, Qingdao
 182 Juchuang Environmental Company, China), and a gas chromatograph (GC2014C with
 183 TCD and TDX-01, Shimadzu Company, Japan). The methanol-water mixture for
 184 reforming was injected into the microreactor by an injection pump. The methanol for
 185 combustion was injected into microreactor by a peristaltic pump, and air for
 186 combustion was transported into microreactor by air bottle and mass flowmeter. The

187 temperature of the reaction chamber plate for combustion was monitored by the
 188 temperature inspector. The reaction temperature of methanol steam reforming reaction
 189 was determined by the temperature of the reaction chamber plate for combustion. The
 190 temperature of the reaction chamber plate for combustion was controlled by the flow
 191 rate of the methanol and air for combustion. The unreacted methanol and water in the
 192 methanol steam reforming gas were separated using the condensation and the drying
 193 pipes. The flow rate of reaction gas was analyzed by a soap flowmeter. The volume
 194 proportions of CO, CO₂, and H₂ in the reaction gas were determined by a gas
 195 chromatograph.

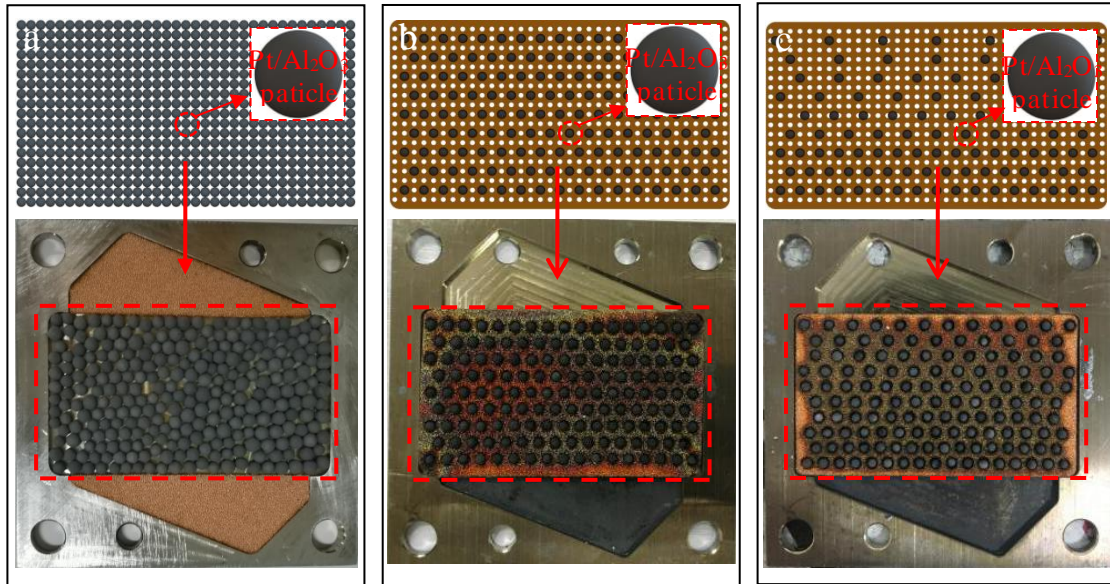
196 After the occurrence of the catalytic combustion reaction in the self-thermal
 197 methanol steam reforming microreactor, the methanol-water mixture was injected into
 198 the microreactor. Then, the methanol steam reforming reaction for hydrogen
 199 production was occurred in the microreactor. The methanol conversion, H₂ flow rate
 200 and CO selectivity were used as indices for evaluating the methanol steam reforming
 201 reaction performance of the microreactor for hydrogen production. Eqs. (5), (6) and (7)
 202 are the empirical formulas for calculating methanol conversion and H₂ flow rate and
 203 CO selectivity^[6,7,25].

$$X_{CH_3OH} = \frac{V_{\text{reaction gas}} * (m + n)}{V_{\text{injection}} * \frac{1}{60} * \frac{1}{64} * \frac{273}{K} * 22400} \quad (5)$$

$$V_{H_2} = \frac{V_{\text{reaction gas}} * z}{22400 * 60} \quad (6)$$

$$S_{co} = \frac{m}{m + n} \times 100\% \quad (7)$$

207 **2.5 Structural design and reaction performance investigation of porous reaction**
208 **support for methanol catalytic combustion**



209
210 Fig.5. Structural diagram of porous reaction supports with different structural designs: (a) A-type;
211 (b) B-type; (c) C-type structures

212 Fig.5 shows the structural diagram of porous reaction supports with different
213 structural designs. Here, Pt/Al₂O₃ spherical catalyst particles with 2 mm external
214 diameter and 1% Pt content were used. A rectangular chamber filled with Pt/Al₂O₃
215 catalyst particles and two oblique chambers filled with 110 PPI copper foam in the
216 reaction chamber plate for combustion were used as catalytic combustion reaction
217 support with A-type structure. The rectangular chamber filled with 110 PPI copper
218 foam and the Pt/Al₂O₃ catalyst particles, which were on the 110 PPI copper foam, in
219 uniform gap distribution, were used as catalytic combustion reaction support with
220 B-type structure. The rectangular chamber filled with 110 PPI copper foam and the
221 Pt/Al₂O₃ catalyst particles, which were on the 110 PPI copper foam, in gradient gap
222 distribution were used as catalytic combustion reaction support with C-type structure.

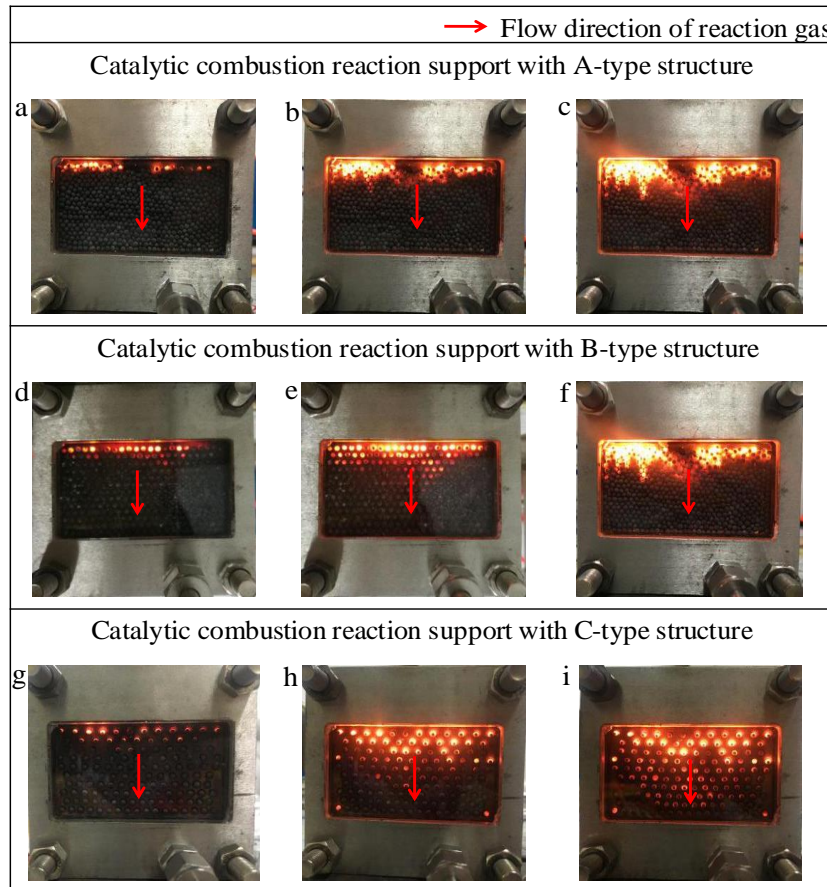
223 The molar ratio of methanol to air in the methanol catalytic combustion reaction
224 was fixed at 0.14. The methanol catalytic combustion reaction performance of the
225 microreactor with the different catalytic combustion reaction supports was studied
226 under 0.26mL/min, 0.78mL/min and 1.3mL/min injection rates of liquid methanol,
227 respectively. Moreover, a small amount (0.5 g) of Cu/Zn/Al/Zr catalyst was loaded on
228 the 110 PPI copper foam of the self-thermal methanol steam reforming microreactor.
229 The reaction performance of the self-thermal methanol steam reforming microreactor
230 with different catalytic combustion reaction supports was investigated under different
231 self-thermal temperatures with 10 mL/h injection rate of methanol-water mixture.

232 **3. Results and discussion**

233 **3.1 Methanol catalytic combustion reaction performance of microreactor**

234 Fig.6 shows an optical image of methanol combustion for porous reaction
235 supports with different structures. The brightness of the flame in the reaction chamber
236 plate for combustion increases with increasing methanol and air flow rates. Moreover,
237 compared with A-type and B-type catalytic combustion reaction supports, the
238 brightness differences in flames at different locations on the reaction chamber for
239 combustion with C-type support were little. Following an increase in methanol and air
240 flow rates, the amount of reaction gas for methanol catalytic combustion increased.
241 Consequently, more exothermic quantity was generated from the methanol catalytic
242 combustion reaction and the more flames in the reaction chamber for combustion
243 were arose. In the C-type support, the front of the reaction chamber plate for
244 combustion had less catalyst particles than the back of the reaction chamber plate to

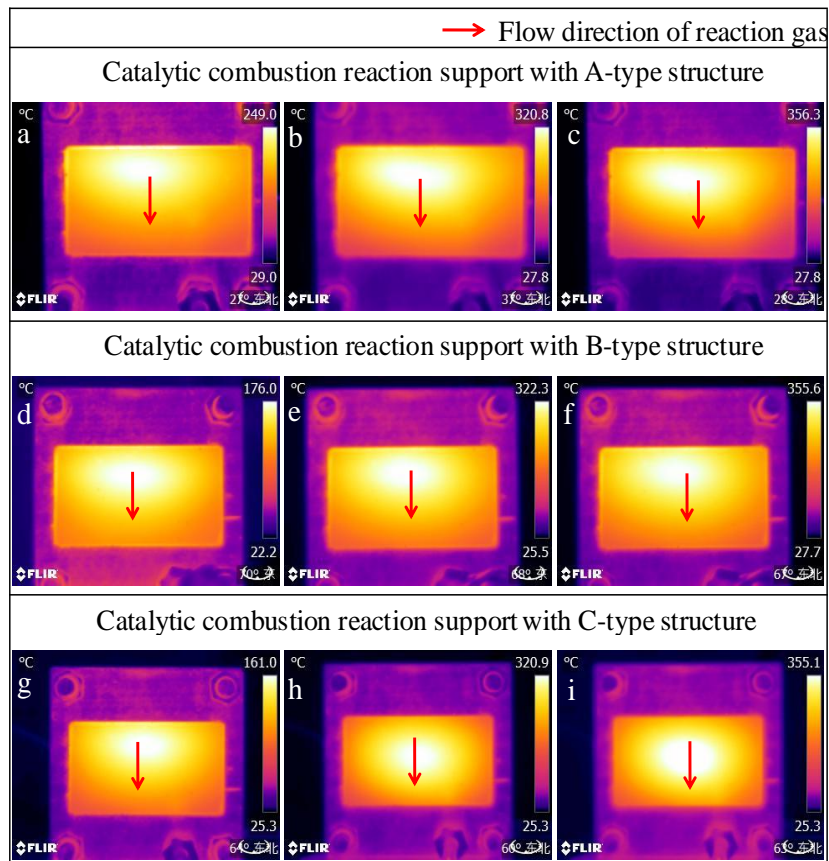
245 prevent overreaction of reaction gas in the front of the reaction chamber plate and
246 reduce the temperature differences between various locations on the reaction chamber
247 plate^[15].



248
249 Fig.6. Optical image of methanol combustion for porous reaction supports with different structures.
250 Catalytic combustion reaction support with A-type structure under different injection rates of
251 methanol: (a) 0.26 mL/min, (b) 0.78 mL/min and (c) 1.3 mL/min. The next three correspond to
252 catalytic combustion reaction support with B-type structure under different injection rates of
253 methanol: (d) 0.26 mL/min, (e) 0.78 mL/min and (f) 1.3 mL/min. Finally, the catalytic combustion
254 reaction support with C-type structure under different injection rates of methanol: (g) 0.26 mL/min,
255 (h) 0.78 mL/min and (i) 1.3 mL/min.

256 Fig.7 shows the infrared thermography of methanol combustion for porous
257 reaction supports with different structures. Compared with A-type and B-type
258 catalytic combustion reaction supports, the thermal distribution region with relatively
259 high temperature for C-type support was closer to the centre of the reaction chamber

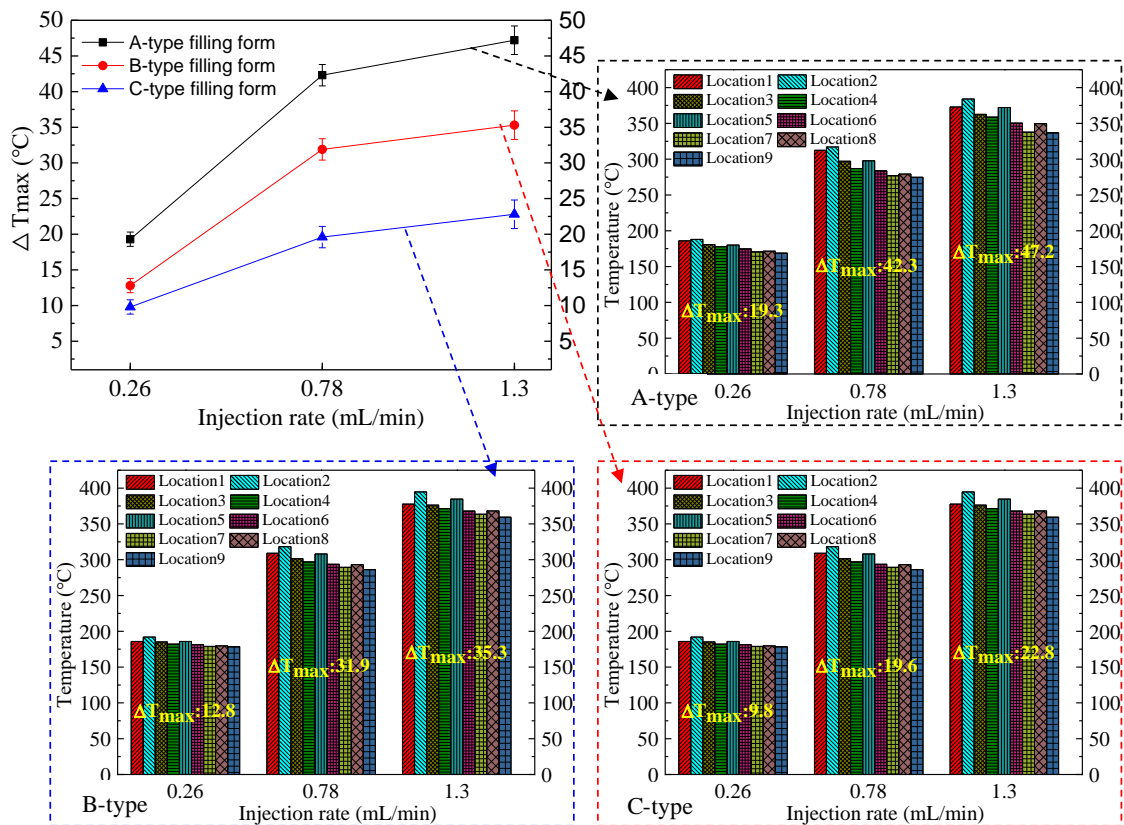
260 for combustion. Moreover, the thermal distribution region with a relatively high
 261 temperature was larger. It was shown that the thermal distribution of the reaction
 262 chamber plate for combustion can be controlled by changing the catalyst distribution
 263 in the reaction chamber plate.



264 Fig.7. Infrared thermography of methanol combustion for porous reaction supports with different
 265 structures. Catalytic combustion reaction support with A-type structure under different injection
 266 rates of methanol: (a) 0.26 mL/min, (b) 0.78 mL/min and (c) 1.3 mL/min. Then, in the B-type
 267 structure under different injection rates of methanol: (d) 0.26 mL/min, (e) 0.78 mL/min and (f) 1.3
 268 mL/min. Finally, in the C-type structure under different injection rates of methanol are shown: (g)
 269 0.26 mL/min, (h) 0.78 mL/min and (i) 1.3 mL/min.
 270

271 Fig.8 shows the maximum temperature differences of thermal distribution on the
 272 reaction chamber plate for combustion with different catalytic combustion reaction
 273 supports. Compared with A-type and B-type supports, the maximum temperature
 274 difference of thermal distribution (ΔT_{\max}) between nine locations of the reaction

275 chamber plate for combustion with C-type support was lower under different injection
 276 rates. The values of ΔT_{\max} of A-type, B-type and C-type support structures were
 277 47.2°C, 35.3°C and 22.8°C, respectively. Compared with A-type structure, the ΔT_{\max}
 278 of C-type support was decreased by 24.4°C. These were compared to examine the fact
 279 that the temperature difference of thermal distribution on the reaction chamber plate
 280 for combustion can be decreased using the C-type catalytic combustion reaction
 281 support. It can be concluded that the gradient gap distribution of Pt/Al₂O₃ catalyst
 282 particles on the 110 PPI copper foam was beneficial for decreasing the ΔT_{\max} of
 283 thermal distribution on the reaction chamber plate for combustion.



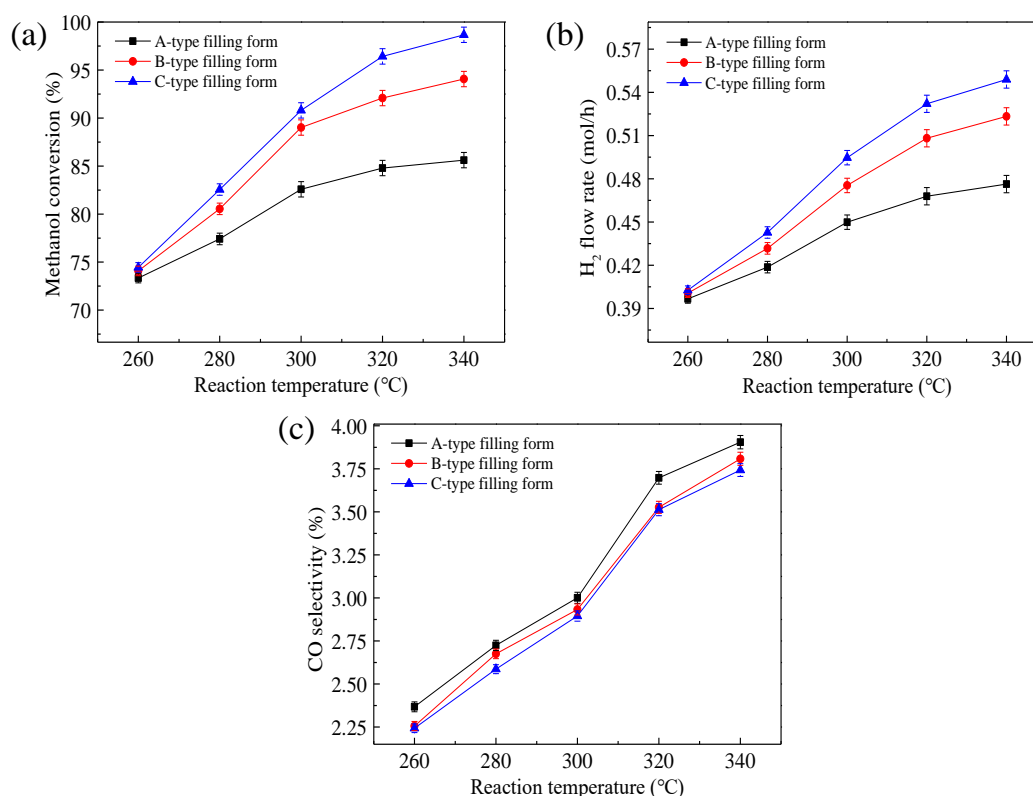
284 Fig.8. Maximum temperature differences of thermal distribution on the reaction chamber plate
 285 for combustion with different catalytic combustion reaction supports
 286

287

288 **3.2 Reaction performance of self-thermal methanol steam reforming**
289 **microreactor**

290 Fig.9 shows the reaction performance in hydrogen production of the self-thermal
291 methanol steam reforming microreactor with different catalytic combustion reaction
292 supports under different self-thermal temperatures. By increasing the self-thermal
293 temperature, the methanol steam reforming reaction performance was increased;
294 moreover, the methanol steam reforming reaction performance gap between the
295 microreactors with different catalytic combustion reaction supports widened.
296 Compared with A-type and B-type reaction supports, the reaction chamber plate for
297 combustion with C-type support exhibited a better methanol steam reforming reaction
298 performance. Especially, compared with A-type, methanol conversion of C-type
299 support was increased by 15.2%, the H₂ flow rate was increased by 15.2% under 10
300 mL/h methanol-water mixture injection rate and 340 °C reaction temperature.
301 Meanwhile, the CO selectivity was decreased by 4.1%. It was shown that Compared
302 with the high value of ΔT_{max} of thermal distribution on the reaction chamber plate
303 for combustion, the smaller value was beneficial for increasing the methanol steam
304 reforming reaction performance of self-thermal microreactor. Compared with A-type
305 and B-type reaction support, the temperature difference of thermal distribution on the
306 reaction chamber plate with C-type support for combustion was smaller. Accordingly,
307 the temperature difference of thermal distribution on the reaction chamber plate for
308 reforming was smaller. Thus the problem of local catalyst deactivation caused by
309 local high temperature will not occur in the reaction chamber plate for reforming^[26-29].

310 In this way, the overall catalytic performance of the catalyst in the reaction chamber
311 plate for reforming will be better^[13]. Therefore, the self-thermal microreactor
312 exhibited a better methanol steam reforming reaction performance in hydrogen
313 production.



314
315 Fig.9. Reaction performance in hydrogen production of the self-thermal methanol steam reforming
316 microreactor with different catalytic combustion reaction supports under different self-thermal
317 temperatures: (a) Methanol conversion, (b) H₂ flow rate, (c) CO selectivity.

318 4. Conclusions

319 Combined with the previous research works of the methanol steam reforming
320 microreactor, a methanol catalytic combustion microreactor, a self-thermal methanol
321 steam reforming microreactor for hydrogen production and the corresponding testing
322 systems were developed. Moreover, the catalytic combustion reaction supports with
323 different structures were designed and manufactured. Furthermore, the related

324 experiments were done. It was found that the developed self-thermal microreactor for
325 hydrogen production can replace traditional electrical heating mode by using
326 methanol catalytic combustion as the heat-supply of the methanol steam reforming
327 reaction. Moreover, compared with A-type support, the ΔT_{\max} of C-type support was
328 decreased by 24.4°C. The thermal distribution of the reaction chamber for combustion
329 can be controlled by changing the catalyst distribution in the reaction chamber plate.
330 Compared with A-type support, the methanol conversion and H₂ flow rate of the
331 self-thermal microreactor with C-type porous reaction support were increased by
332 15.2% under 10 mL/h methanol-water mixture injection rate and 340 °C self-thermal.
333 Meanwhile, the CO selectivity was decreased by 4.1%. It can be concluded that the
334 gradient gap distribution of Pt/Al₂O₃ catalyst particles on the 110 PPI copper foam
335 was beneficial for decreasing the ΔT_{\max} of thermal distribution on the reaction
336 chamber plate for combustion. Compared with the high value of ΔT_{\max} of thermal
337 distribution on the reaction chamber plate for combustion, the smaller value was
338 beneficial for increasing the methanol steam reforming reaction performance of
339 self-thermal microreactor.

340 **Acknowledgments**

341 This work was supported by the National Natural Science Foundation of China
342 (Nos.51975496 and 51922092), the Natural Science Foundation of Fujian Province of
343 China (No.2017J06015) and Guangdong Natural Science Funds for Distinguished
344 Young Scholars (No.2016A030306032). Moreover, the supports from Xiamen
345 University and the Fundamental Research Fund for Central Universities

346 (No.20720180076) are also acknowledged.

347 **References**

348 [1] Dincer I, Acar C. Review and evaluation of hydrogen production methods for
349 better sustainability. *Int J Hydrogen Energy*. 2015;34:11094-111.

350 [2] Wang F, Cao YD, Wang GQ. Thermoelectric generation coupling methanol steam
351 reforming characteristic in microreactor. *Energy*. 2015;80:642-53.

352 [3] Gholami A, Pourfayaz F, Hajinezhad A, Mohadesi M. Biodiesel production from
353 Norouzak (*Salvia leriifolia*) oil using choline hydroxide catalyst in a microchannel
354 reactor. *Renew Energ*. 2019;136:993-1001.

355 [4] Tian JS, Ke YZ, Kong GG, Tan MW, Wang Y, Lin JD, et al. A novel structured
356 PdZnAl/Cu fiber catalyst for methanol steam reforming in microreactor. *Renew*
357 *Energ*. 2017;113:30-42.

358 [5] Mei DQ, Qian M, Yao ZH, Liu BH, Lou XY, Chen ZC. Effects of structural
359 parameters on the performance of a micro-reactor with micro-pin-fin arrays (MPFAR)
360 for hydrogen production. *Int J Hydrogen Energy*. 2012;37:17817-27.

361 [6] Zhou W, Yu W, Ke YZ, Liu YX, Wan SL, Lin JD. Size effect and series-parallel
362 integration design of laminated methanol steam reforming microreactor for hydrogen
363 production. *Int J Hydrogen Energy*. 2018;43:19396-404.

364 [7] Zhou W, Ke YZ, Wang QH, Wan SL, Lin JD, Zhang JP, et al. Development of
365 cylindrical laminated methanol steam reforming microreactor with cascading metal
366 foams as catalyst support. *Fuel*. 2017;191:46-53.

367 [8] Rath R, Kumar P, Mohanty S, Nayak, SK. Recent advances, unsolved deficiencies,
368 and future perspectives of hydrogen fuel cells in transportation and portable sectors.
369 *Int J Energ Res*. 2019;15:8931-55.

370 [9] Gu XG, Taylor RA, Li Q, Scott JA, Rosengarten G. Thermal analysis of a micro
371 solar thermal collector designed for methanol reforming. *Solar Energy*.
372 2015;113:189-98.

373 [10] Tanaka SJ, Chang KS, Min KB, Satoh D, Yoshida K, Esashi M. MEMS-based

374 components of a miniature fuel cell/fuel reformer system. Chem Eng J.
375 2004;101:143-49.

376 [11] Chein RY, Chen YC, Chen JY, Chung JN. Design and test of a miniature
377 hydrogen production reactor integrated with heat supply, fuel vaporization,
378 methanol-steam reforming and carbon monoxide removal unit. Int J Hydrogen
379 Energy. 2012;37:6562-71.

380 [12] Hsueh CY, Chu HS, Yan WM, Chen CH. Numerical study of heat and mass
381 transfer in a plate methanol steam micro reformer with methanol catalytic combustor.
382 Int J Hydrogen Energy. 2010;35:6227-38.

383 [13] Herdem MS, Mundhwa M, Farhad S, Hamdullahpur F. Multiphysics modeling
384 and heat distribution study in a catalytic microchannel methanol steam reformer.
385 Energy Fuel. 2018;32:7220-34.

386 [14] Wang F, Wang GQ. Performance and cold spot effect of methanol steam
387 reforming for hydrogen production in micro-reactor. Int J Hydrogen Energy.
388 2016;41:16835-41.

389 [15] Zheng TQ, Zhou W, Yu W, Ke YZ, Liu YX, Liu RL, Kwan SH. Methanol steam
390 reforming performance optimisation of cylindrical microreactor for hydrogen
391 production utilising error backpropagation and genetic algorithm. Chem Eng J. 2019;
392 357:641-54.

393 [16] Chen WH, Shen CT, Lin BJ, Liu SC. Hydrogen production from methanol partial
394 oxidation over Pt/Al₂O₃ catalyst with low Pt content. Energy. 2015;88:399-407.

395 [17] Alvarez-Galvan MC, Navarro RM, Rosa F, Briceño Y, Ridao MA, Fierro JLG.
396 Hydrogen production for fuel cell by oxidative reforming of diesel surrogate:
397 Influence of ceria and/or lanthana over the activity of Pt/Al₂O₃ catalysts. Fuel.
398 2008;87:2502-11.

399 [18] Parmar RD, Kundu A, Thurgood C, Peppley BA, Karan K. Kinetic studies of the
400 autothermal reforming of tetradecane over Pt/Al₂O₃ catalyst in a fixed-bed reactor.
401 Fuel. 2010;89:1212-20.

402 [19] Luo YJ, Xiao YH, Cai GH, Zheng Y, Wei K. Performance of Ce_{0.25}Zr_{0.75}O₂
403 promoted Pd/Ag/c-Al₂O₃ catalysts for low-temperature methanol oxidation. Fuel.

404 2012;93:533-38.

405 [20] Fu BR, Ting YC, Lee CF, Huang YJ, Su YC, Tseng FG, Pan C. Real-time
406 monitoring of a micro reformer integrated with a microchannel heat exchanger by
407 infrared thermography and high-speed flow images. *Int J Hydrogen Energy*.
408 2016;41:18610-20.

409 [21] EI-Amiri A, Saifi A, Elhassnaoui A, Obbadi A, Errami Y, Sahnoun S.
410 Control of solid oxide fuel cells damage using infrared thermography. *Int J Hydrogen*
411 *Energy*. 2020;45:11695-703.

412 [22] Park GG, Seo DJ, Park SH, Yoon YG, Kim CS, Yoon WL. Development of
413 microchannel methanol steam reformer. *Chem Eng J*. 2004;101:87-92.

414 [23] Yu H, Chen H, Pan M, Tang Y, Zeng K, Peng F, et al. Effect of the metal foam
415 materials on the performance of methanol steam micro-reformer for fuel cells. *Appl*
416 *Catal A-Gen*. 2007;327:106-13.

417 [24] Mei DQ, Feng YB, Qian M, Chen ZC. An innovative micro-channel catalyst
418 support with a micro-porous surface for hydrogen production via methanol steam
419 reforming. *Int J Hydrogen Energy*. 2016;41:2268-77.

420 [25] Zheng TQ, Zhou W, Geng D, Li YY, Liu YX, Zhang CY. Methanol steam
421 reforming microreactor with novel 3D-Printed porous stainless steel support as
422 catalyst support. *Int J Hydrogen Energy*. 2020;45:14006-16.

423 [26] Twigg MV, Spencer MS. Deactivation of supported copper metal catalysts for
424 hydrogenation reactions. *Appl Catal A-Gen*. 2001; 212:161-74.

425 [27] Ajamein H, Haghghi M, Shokrani R, Abdollahifar M. On the solution
426 combustion synthesis of copper based nanocatalysts for steam methanol reforming:
427 Effect of precursor, ultrasound irradiation and urea/nitrate ratio. *J Mol Catal A-Chem*.
428 2016;421:222-34.

429 [28] Minaei S, Haghghi M, Jodeiri N, Ajamein H, Abdollahifar M. Urea-nitrates
430 combustion preparation of CeO₂-promoted CuO/ZnO/Al₂O₃ nanocatalyst for fuel cell
431 grade hydrogen production via methanol steam reforming. *Adv Powder Technol*.
432 2017;28:842-53.

433 [29] Zhu QF, Zhang QC, Wen LX. Anti-sintering silica-coating CuZnAlZr catalyst for

434 methanol synthesis from CO hydrogenation. *Fuel Process Technol.* 2017;156:280-89.